Applied Catalysis B: Environmental 257 (2019) 117847

Contents lists available at ScienceDirect

Applied Catalysis B: Environmental

journal homepage: www.elsevier.com/locate/apcatb

Intelligent catalytic support by Ni / NiO / $Ni(OH)_2$ in low level of Pd/Pt boosting the performance of alkaline DEFC

Abhijit Dutta[a,b,*], Rajib Adhikary[c], Peter Broekmann[a], Jayati Datta[b,c,*]

[a] Department of Chemistry and Biochemistry, University of Bern, Freistrassee 3, Bern, 3012, Switzerland
[b] Electrochemistry & Fuel Cell Laboratory, Department of Chemistry, Indian Institute of Engineering Science and Technology, Shibpur, Howrah, 711 103, West Bengal, India
[c] Department of Chemistry, Renewable Energy Research Center, Heritage Institute of Technology, Kolkata, 700107, West Bengal, India

ARTICLE INFO

Keywords:
Nano catalyst
NiPdPt
EOR
Power density
Products analysis

ABSTRACT

The present investigations explore the important contribution of transitional metal/metal oxide/hydroxide in ternary alloys of Ni, Pd, and Pt NPs for boosting the EOR in alkaline DEFCs. A facile one-pot synthesis method is employed to prepare ultra small ternary nano-alloy catalysts. The impact of Ni/NiO /$Ni(OH)_2$ species in EOR on Pd/Pd catalyst is strongly recognized by the diminution of overvoltage ~ 546 mV in case of the multi metallic surface. The oxy/hydroxy species of the multi-metallic formulation of $Ni_{29}Pd_{34}Pt_{37}$ not only trigger the electrode kinetics at the lower electro-chemical bias-potential but also facilitate towards sustained product formation and electro-extraction as manifested by the output power. A substantial rise of peak power density is obtained by more than 241% higher as compared to Pt, 78%, and 51%, compared to the bimetallic $Ni_{41}Pt_{59}$ and $Pd_{55}Pt_{45}$ catalysts, respectively. The increase of $CH_3CO_2^-$ and CO_3^{2-} yields on the ternary catalyst compared to its unary/binary counterparts, further confirms the catalytic preeminence of the combinatorial formulation of $Ni_{29}Pd_{34}Pt_{37}$ in the present investigation.

1. Introduction

Since the recent past, partially alloyed and also alternative catalyst nano particles (NPs) has over taken the concept of using high loading of Pt for the DEFCs. This also relates to the relatively less abundance, limited affordability and poisoning intolerance of the single Pt catalyst for the alcohol oxidation reaction in fuel cells [1–3]. In fact success in electro-catalysis of the alloy materials in propagating the alcohol oxidation lies with the attributes of bi-functional mechanism [4,5] and the electronic effect [6–8] persuaded by the electronic interaction of Pt with the co-metals and this is particularly relevant to the acid environment [9–11]. However, the selective oxidation of alcohols in alkaline solutions is expected to follow somewhat different pathway involving a set of different catalysts formulations [12,13]. Moreover, in recent times with the advent of anion exchange membrane, there has been upsurge of interest in exploring the kinetic advantages of fuel cell reactions in alkaline medium with various cheaper combinations of alloyed/composite materials as efficient catalysts [14]. The spurt for designing multi-metallic catalysts is in fact the consequence of poor performances of the monometallic catalysts. The multi-metallic ensembles bear the advantage of the promoting the electronic and electrochemical properties by the conjugate lattice parameters, size control and complimentary catalytic activity of the ad-atoms [7,10,15–17].

The rate of breaking the C—C bond in higher alcohols like ethanol strongly depends on the degree of its interaction of the reactant molecule with the adsorption sites of the catalyst and the kinetics of electron transfer. Based on the above aspects, several bimetallic catalysts such as Pt-Ni, Pt-Cr, Pt-Au and Pt-Co, *etc* have been reported for the study of kinetics and mechanism of ethanol oxidation reaction (EOR) [7,17–20]. A series of oxide-promoted binary catalysts have also been reported showing improved activities towards the EOR in alkaline media [9,21–23]. Carbon-supported PtAu and PtSn catalysts showed higher current density and long-term stability in ethanol oxidation in alkaline solution [24,25]. Pt alloyed with Pd and/or Ni has arisen wide attraction in recent years [26–29]. The metallic surface segregation was found in a pure Pt surface atomic layer in PtNi catalysts [16,30,31]. For the catalysts enriched with Ni as ad-atoms, the subsurface atomic layers are enriched with electronic as well as catalytically active reaction sites by coverage of oxy/hydroxyl species. The morphology of the catalyst matrix, atomic structure of the PtNi (111) surface and stability are therefore of utmost importance while examining the origin of its increased activity for ethanol oxidation reaction [7,29,32].

In course of synthesizing anode materials, attempts are being made to add a third component to the respective binary matrix. Zhou et al.

* Corresponding authors.
E-mail addresses: abhijit.dutta@dcb.unibe.ch (A. Dutta), jayati_datta@rediffmail.com (J. Datta).

https://doi.org/10.1016/j.apcatb.2019.117847
Received 8 November 2018; Received in revised form 4 June 2019; Accepted 7 June 2019

reported the catalytic superiority towards EOR on Pt–based, PtRuW and PtRuMo catalyst and showed excellent behavior in acid medium [33]. Furthermore, Pt based binary and ternary catalysts deposited onto the Au substrate by Tenka et al. and $Pt_6Ru_3Ni_1/C$, Pt_1Ru_1/C were tested by Wang et al. as catalysts for ethanol oxidation in acid media [34,35]. However, there are couples of reports on potential ternary catalysts for ethanol electro-oxidation for the alkaline DEFCs [5–7,25,29,36,37]. Hence, a major thrust may be given to study the catalytic activity of the multi-metallic nano-ensembles toward promoting EOR kinetics and better selectivity toward ultimate formation of oxidation products in alkaline media. *Therefore, in pursuit of exploiting transitional metal/metal oxide (Ni/NiO/Ni(OH)$_2$) based catalyst formulation*, the present study focus on the fabrication of EOR catalyst with Pd/Pt base to form the binary skeleton structure decorated with Ni/NiO/Ni(OH)$_2$ entities by simultaneous $NaBH_4$ reduction method and arriving at the ternary catalyst composition. The synthesized nano-structured unary Pt/C, binary PdPt/C, NiPt/C, and ternary NiPdPt/C catalysts were compared in terms of their electro-catalytic performances towards EOR. The kinetic parameters and the apparent activation energy towards EOR were determined within the temperature range of 20 − 80 °C. A strong correlation between the functional properties of the co-metals was made by the help of morphology, and compositional analysis of the catalyst NPs and their electrochemical performances. Ion-chromatography was employed to estimate oxidation products formed during electrolysis. The relative quantity of acetates and carbonate yields on catalysts matrices reflects the electron extraction pathway and the electrochemical sustenance towards ultimate decomposition of ethanol. The electrical performance of the anodic reaction was studied using the synthesized catalysts assembled with anion-exchange membrane (AEM) in an 'in-house' fabricated DEFC at an intermediate temperature of 40 °C.

2. Result and discussion

2.1. Structural characterization

The multimetallic (ternary and binary) NPs were synthesized (see supplementary information file for the preparation of NPs by one pot wet chemical reduction process) and loaded on vulcan carbon (40%) during the reduction of the metals precursor. In order to quantify the exact metal loading with respect to the carbon supports, thermal gravimetric analysis (TGA) has been carried out (vide Table S1 in supplementary information file). The chemical compositions of the NiPdPt/C, PdPt/C and NiPt/C catalysts were also determined by EDX and ICP-AES analysis. Typical compositional analyses in terms of atomic percent are summarized in Table S1 in supplementary information. The crystalline structure and the lattice properties of the catalysts were determined by means of X ray diffraction analysis. Fig.1a shows characteristic XRD patterns for Pt/C, $Pd_{55}Pt_{45}/C$, $Ni_{41}Pt_{59}/C$, and $Ni_{29}Pd_{34}Pt_{37}/C$ catalysts. The diffraction peaks can be indexed as (111), (200), (220), (311), and (222) reflections of the fcc structure. The close inspection of the peak positions discloses minor differences in terms of lattice parameters (vide Table S1 in supplementary information file). For unary metal NPs, 2θ values are 39.7 (111), 46.3 (200), and 67.3 (220) for Pt; 44.5 (111), 51.8 (200), and 76.3 (220) for Ni and 40.1 (111), 46.6 (200), and 68.1 (220) for Pd). It is found that the diffraction planes (111) for the $Pd_{55}Pt_{45}/C$, $Ni_{41}Pt_{59}/C$ and $Ni_{29}Pd_{34}Pt_{37}/C$ catalysts are shifted to the respective higher 2θ angles (41.59, 40.13, and 40.37), in comparison with the database of (111) unary metal NPs. This is better discernable in the magnified image (Fig. 1b) and is indicative of the reduction of the lattice constant in the catalyst matrices. Similar trend also follows for 2θ of the (220) peaks [67.71 (Pt), 70.11 ($Ni_{41}Pt_{59}/C$), 68.46 ($Pd_{55}Pt_{45}/C$), 68.64 ($Ni_{29}Pd_{34}Pt_{37}/C$)]. There are no peaks corresponding to fcc Ni metals or oxides/hydroxides found in the diffraction patterns. The peak shift to higher angle for Pt, accounts for the alloy formation in between Pt, Ni and Pd [16,28,29,38,39]. The higher peak shifts in $Ni_{41}Pt_{59}/C$ compared to $Pd_{55}Pt_{45}/C$ suggest better alloying in case of Ni-Pt combination. The d spacing of (111) in the $Ni_{41}Pt_{59}/C$, $Pd_{55}Pt_{45}/C$ and $Ni_{29}Pd_{34}Pt_{37}/C$ NPs are 2.23 Å, 2.24 Å and 2.22 Å, respectively, whereas those of pure Pt and Ni are 2.260 Å and 2.034 Å. The resulting patterns reveal only the characteristic diffraction peaks of the Pt fcc structure, as discussed earlier. Comparing with the (111) reflection of Pt/C alone, the $Ni_{29}Pd_{34}Pt_{37}/C$ nano-catalyst prepared with different molar ratios of Ni :Pd: Pt displayed as usual the diffraction patterns similar to those of the Pt, except that the 2θ values were again shifted to slightly higher values possibly due to the fact that

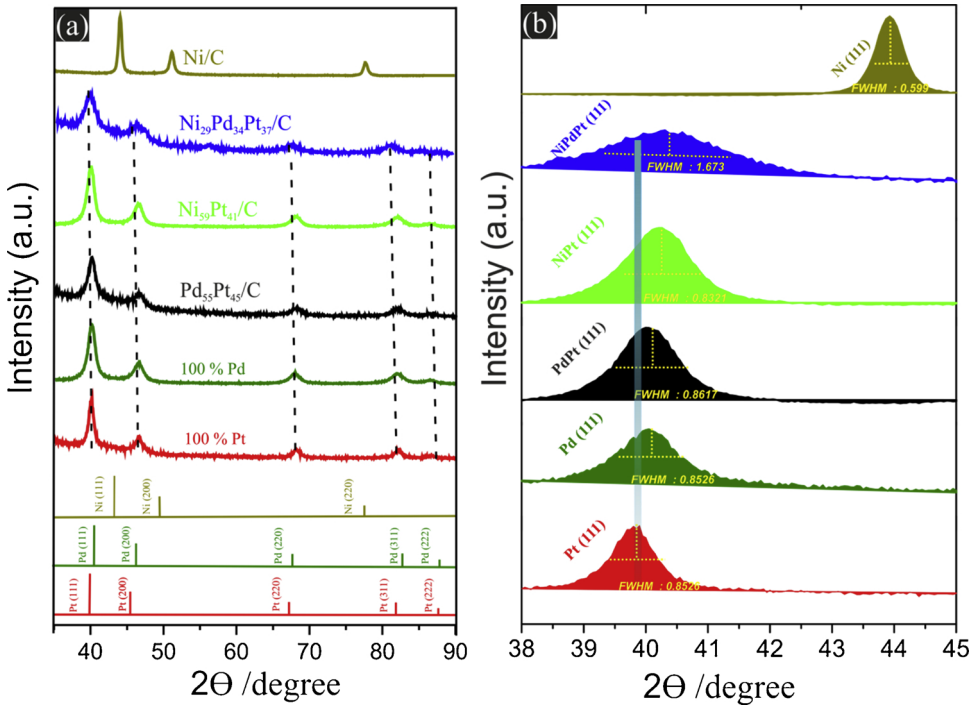

Fig. 1. (a) XRD diffractograms of NiPtPt/C, NiPt/C, Pd/PtC, Pd/C, Pt/C and Ni/C catalysts. **(b)** Magnified view of the (111) XRD peak.

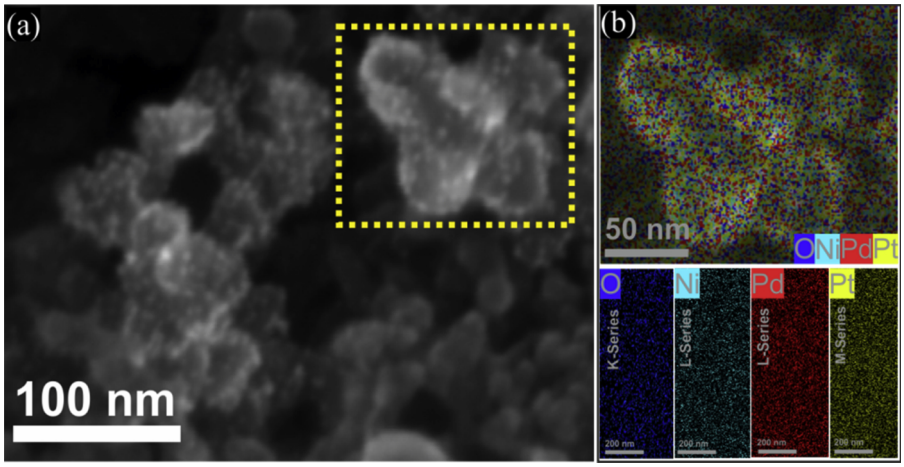

Fig. 2. (a) High resolution (HR) SEM images and (b) elemental mapping of $Ni_{29}Pd_{34}Pt_{37}$/ NPs. The corresponding atomic orbital lines were shown in lower panel (b).

the catalysts have single-phase-disordered structures. The peaks corresponding to the typical hcp structure of pure Ni or NiO/ $Ni(OH)_2$ were not detected in the XRD pattern of ternary matrix. However, as expected, the NiPdPt alloys have metallic Ni and Pd in the Pt lattice, also the metallic grains are intermixed with amorphous Ni oxides, such as NiO, Ni (OH) $_2$, and NiOOH which have been latter detected by XPS analysis [28,32]. The contraction in the lattice parameters of the NiPdPt/C catalysts further reflects the incorporation of Pd and Ni into the alloyed state with Pt.

The crystallite sizes of the unary, binary and ternary catalyst have been calculated according to the Scherrer formula ($L = 0.9\lambda / \beta \cos\theta$, L = crystallite size, β= full width of diffraction line at half its maximum intensity (radians) for deriving particle size. Thus we see that β and L are reciprocally related: the greater the broadening (FWHM) the smaller the crystallite size and vice-versa (see Fig.1b for FWHM value). The FWHM increases with addition of the 3rd metal (Ni) in the binary matrix (PdPt), shown Fig1b. However, an important point to be mentioned that the Scherrer equation does not consider the strain effect in the calculation of the crystallites size which may also possibly affect the peak broadening and/or shifting of crystallites. In addition, the possible strain effects in the binary/ternary system due to the addition of other metals may also play a role for the peak broadening/shifting in XRD peaks. The addition of one or more metals causes homogeneous strain which may be responsible for changing the diffraction parameters d, λ, θ given in Bragg's Law. If the crystallite is strained then the d spacing (lattice plane) will be changed; a compressive and tensile stress could make the d spacing smaller and larger, respectively. Considering the decrease of the d spacing due to homogeneous/inhomogeneous strain the given spacing will be decreased and consequently, the position of the peak will increase from 2θ. Furthermore, the crystallite in the binary and ternary matrix were strained (compressed), resulting in the lattice contraction which is reflected in the peak shift to higher 2θ value. This might happen during formation of alloying structure with addition of one or more metals crystallites. In our case, the addition of Pd or Ni to the Pt matrix causes the peak shifting and at the same time the lattice parameter decreases in PdPt or NiPt compared to Pt (3.913 Å) (see Table S1 in supplementary file).Furthermore, if the strain is inhomogeneous then different crystallites are affected by strain in different amounts and the 2θ shifts varies and the possible formation of the crystallite containing defects may also results in peak broadening. Thus, the crystallite sizes (particle size) obtained from XRD have been compared with the size obtained from HRTEM for all the catalysts (NiPdPt, NiPt, NiPd, Pd, Pt) shown in later section.

High resolution SEM in combination with elemental mapping analysis of $Ni_{29}Pd_{34}Pt_{37}$/C NPs has been performed and shown in Fig. 2a–b. The analysis shows homogenious distribution of metallic $Ni_{29}Pd_{34}Pt_{37}$/C NPs, containing the Ni, Pd, Pt and oxygen in the electron micrograph (Fig. 2a). The corresponding atomic orbital lines/series were also shown in the lower panel of the Fig.2b.

Representative TEM images of ternary $Ni_{29}Pd_{34}Pt_{37}$/C catalyst show that the NPs are distributed uniformly over the carbon support (Fig. 3a and b). The observed particles are largely characterized by the nano crystalline feature, as observed by close examination of the individual particles grown on the matrix. The corresponding size distribution patterns are displayed (over 200 particles) in the Fig. 3c and the resulting particle size ranging between 3–5 nm. The TEM images and the size distributions of the unary metals (Pt/C, Pd/C) and others binary ($Pd_{55}Pt_{45}$/C and $Ni_{41}Pt_{59}$/C) catalysts have been shown in Figs. S1 and S2, respectively in supplementary information. The SADP shown in Fig. 3d indicates the formation of nanophases of the $Ni_{29}Pd_{34}Pt_{37}$/C catalyst with good crystallinity and the rings are indexed for an fcc crystal structure. A typical fringe pattern in Fig.3e–g shows the crystalline planes of the $Ni_{29}Pd_{34}Pt_{37}$/C NPs. Fringe patterns of the single NPs of $Ni_{29}Pd_{34}Pt_{37}$ having different d-spacing have been magnified from Fig. 3e and included in Fig. S3 in supplimentry file. The interplaner d-spacing has been measured by the assistance of the line profile and the FFT pattern as shown in Fig. 3g (inset) and h respectively. The lattice spacing of unary NPs corresponding to (111) planes of Ni, Pd and Pt are found to be 0.2034 nm, 0.224 nm and 0.226 nm, respectively. Interestingly, the d-spacing of $Ni_{29}Pd_{34}Pt_{37}$/C is shifted to 0.2227 nm from 0.2265 nm (Pt (111) (JCPDS 04-0802)) signifying alloy formation between the three NPs, which is also validated by XRD data. In this investigation the particle size obtained from TEM analysis is found to be slightly larger than those calculated from XRD which is attributed to either the interference of Pt (111) peak with the same crystal structure (fcc) of Pd peaks nearby, resulting in a broadening of Pt (111) diffraction peak or by the contributions from amorphous species, most likely the oxides, on the surface of the tri-metallic particles. It appears that an ensemble of co-metals with the base metal form clusters with optimal size that provides favorable reaction centers throughout the matrix. Furthermore, the integrated elemental composition of the NiPdPt/C alloy catalysts was evaluated by EDX analysis on several different regions of each sample of the carbon supported catalyst particles. Fig.3i shows a representative EDX pattern of the $Ni_{29}Pd_{34}Pt_{37}$/C.

In order to understand the chemical / electronic state of the ternary alloy ($Ni_{29}Pd_{34}Pt_{37}$), XPS analysis has been employed. Fig. 4a–c show the XPS profiles of the nanostructured $Ni_{29}Pd_{34}Pt_{37}$ with signatures of Ni, Pd, and Pt. The $Ni2p_{3/2}$ spectrum reveals a strong satellite signal of high binding energy which is adjacent to the main peaks, characteristic to multi-electron excitation [15,21,23,29,40,41]. The Ni 2p XPS states comprise of metallic Ni and Ni^{+2} species, as shown in Figs. 4a and S3 in supplementary file. The $Ni2p_{3/2}$ XPS band is de-convoluted into four

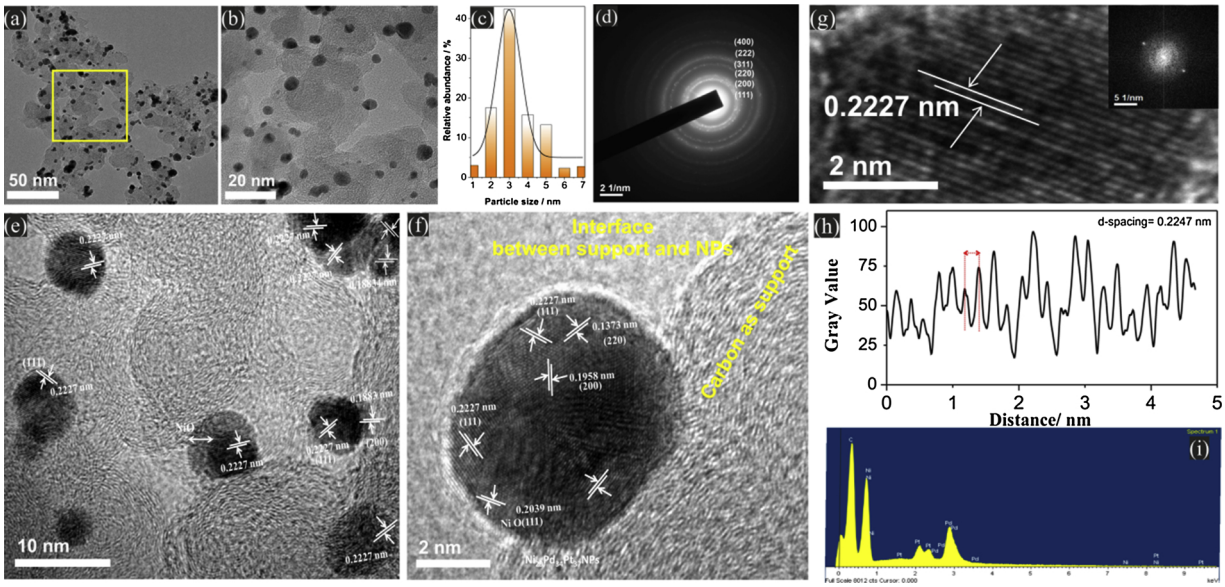

Fig. 3. HRTEM image of $Ni_{29}Pd_{34}Pt_{37}/C$ (a) an overview (b) magnified view of the selected area (c) the particle size distribution (d) SADP pattern of ternary catalyst (e)-(g) HRTEM images and fringe patterns of the single particle having different d-spacing. Inset of (g) FFT pattern and (h) profile line analysis as fingerprints for d-spacing evaluation (i) EDX spectrum of the of $Ni_{29}Pd_{34}Pt_{37}/C$ catalysts.

peaks at 852.8, 853.6, 855.5, and 857.3 eV, corresponding to metallic Ni, NiO, $Ni(OH)_2$ and NiOOH respectively. The area percentages of the respective peaks are 8.57, 15.27, 53.49, and 22.67% as displayed in Fig. 4a. On the other hand, the deconvolution of the XPS band of Pd3d represents an additional low intensity emissions at 335.4 eV and 340.7 eV corresponding to the $3d_{5/2}$ and $3d_{3/2}$, respectively, with a doublet peak energy separation [42,43], suggesting the presence of Pd (II) in small amount (Fig. 4b). The binding energies (BEs) of the Pt

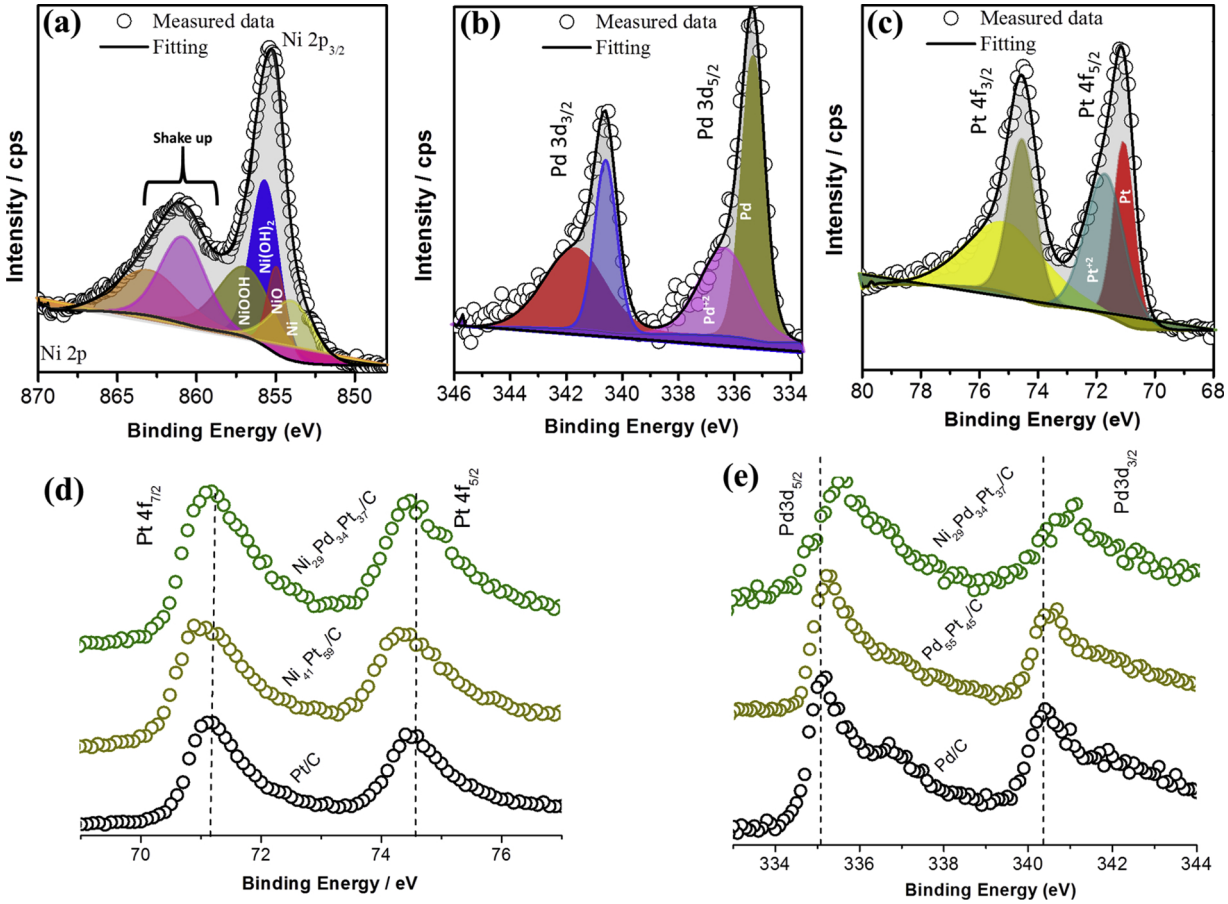

Fig. 4. XPS survey spectrum of $Ni_{29}Pd_{34}Pt_{37}$ternary catalyst (a) Ni (b) Pd and (c) Pt region of the full spectrum; (d) The Pt4f core level XPS spectra of Pt, $Ni_{41}Pt_{59}$ and $Ni_{29}Pd_{34}Pt_{37}$ catalysts (e) The Pd 4f core level XPS spectra of Pd, $Pd_{55}Pt_{45}$ and $Ni_{29}Pd_{34}Pt_{37}$ catalysts.

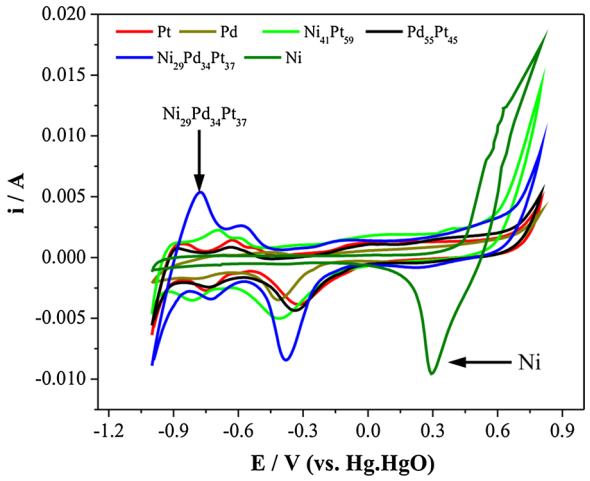

Fig. 5. Cyclic voltammograms of ternary $Ni_{29}Pd_{34}Pt_{37}$, binary $Ni_{41}Pt_{59}$, $Pd_{55}Pt_{45}$, and unary Pt/C, Pd/C and Ni catalysts, recorded in 0.5 M NaOH at sweep rate of 10 mV s^{-1}.T = 25 °C.

region in the ternary catalyst, exhibit similar behavior for the Pt 4f spectra of $4f_{5/2}$ and $4f_{3/2}$ electrons at 72.23 eV and 75.39 eV, respectively, with a shoulder at the higher binding energy side of each peak [44]. Interestingly, the BEs of Pt region is shifted negatively after introduction of Ni in the binary matrix ($Ni_{41}Pt_{59}$) and is further moved after addition with Ni and Pd in the $Ni_{29}Pd_{34}Pt_{37}$/C NPs as shown in Fig. 4d. The shift of the Pt 4f emmision towards lower BEs is possibly due to the addition of Pd and Ni which presumably attributes to the electron transfer taking place from Ni to Pd and Pd to Pt in consequence with the increasing ionization energy of co-metals in the order Ni < Pd < Pt. Moreover, the Pd 3d XPS band in $Pd_{55}Pt_{45}$ and $Ni_{29}Pd_{34}Pt_{37}$ NPs shows higher BEs compared to the unary Pd/C, suggesting electron transfer between the co-metals as shown in Fig. 4e.

2.2. Electrochemical characterization

The electrochemical characteristics of the catalyst-electrolyte interface is demonstrated in Fig. 5 by the voltammetric measurements of Pt/C, Pd/C, $Ni_{41}Pt_{59}$/C, $Pd_{55}Pt_{45}$/C and $Ni_{29}Pd_{34}Pt_{37}$/C catalysts in alkaline medium. Amongst all the catalysts, $Ni_{29}Pd_{34}Pt_{37}$/C bears relatively large electrochemical active surface area (ECSA) as evident from the hydrogen adsorption and desorption peak and also the oxide reduction peak. The presence of Ni and Pd in the Pt matrix therefore has great influence on generating active reaction center throughout the matrix. Both the single Pt and Pd electrodes exhibit suppressed hydrogen and double layer region while pure Ni/C is almost featureless except the oxide reduction region is obtained at a considerable positive potential (Fig.5). The current response in the double layer region of the $Ni_{29}Pd_{34}Pt_{37}$/C electrode becomes broader and at a potential about

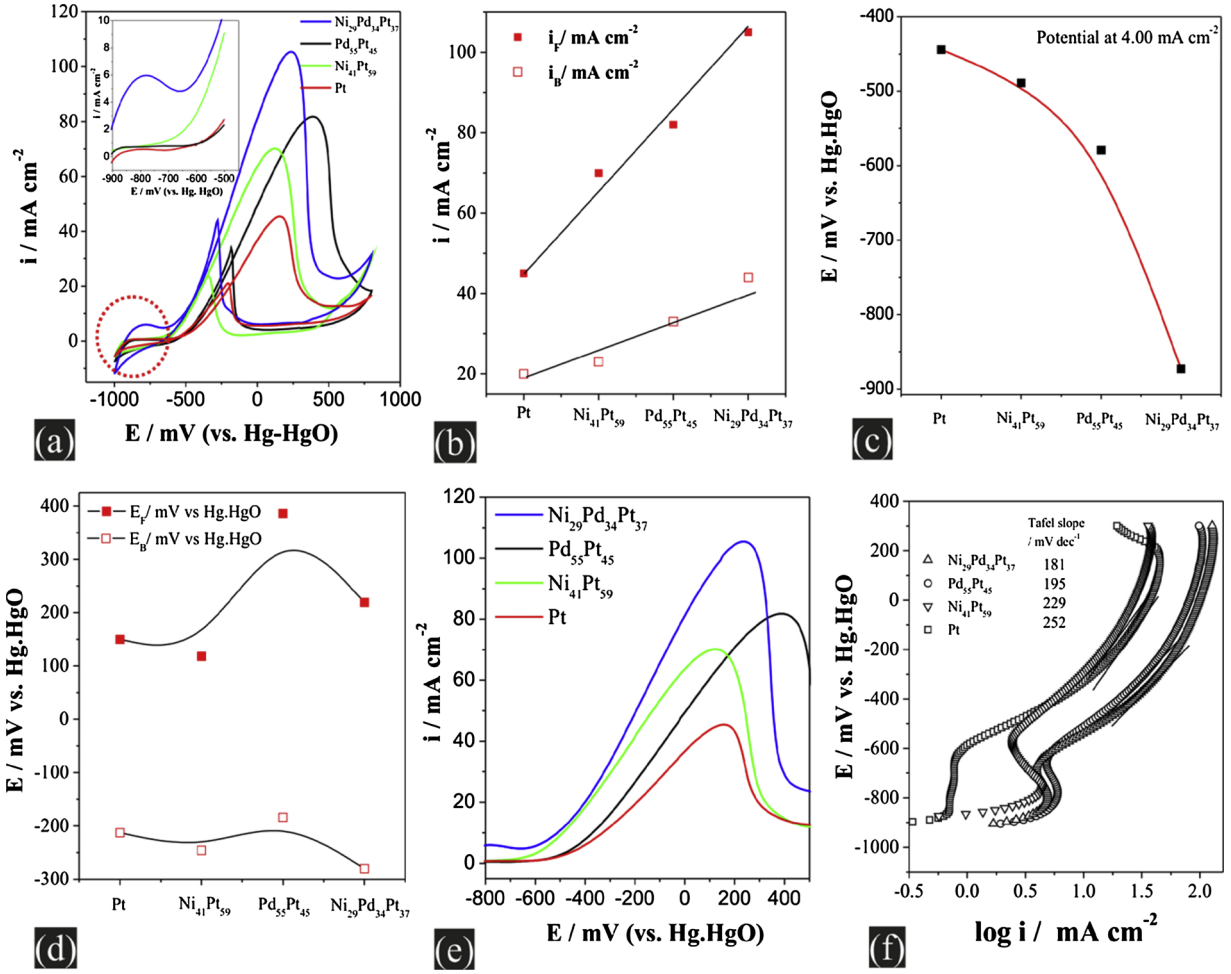

Fig. 6. (a) Cyclic Voltammograms for ethanol oxidation on ternary $Ni_{29}Pd_{34}Pt_{37}$, binary$Ni_{41}Pt_{59}$, $Pd_{55}Pt_{45}$, and unaryPt/C, electrodes in a solution containing 0.5 M NaOH and 1.0 M ethanol at room temperature. Sweep rate: 50 mV s^{-1}. Inset: Magnified view of the onset region of EOR. Plots of (b) forward (I_F) & backward (I_B) current density (c) Potential at 4.00 $mAcm^{-2}$ current regions (d) forward (E_F) & backward (E_B) potential with different electrodes. (e) Potentiodynamic polarisation plots obtained in 1.0 M ethanol and 0.5 M NaOH at a slow scan rate of 10 mV s^{-1} (f) The corresponding Tafel plots of the catalysts.

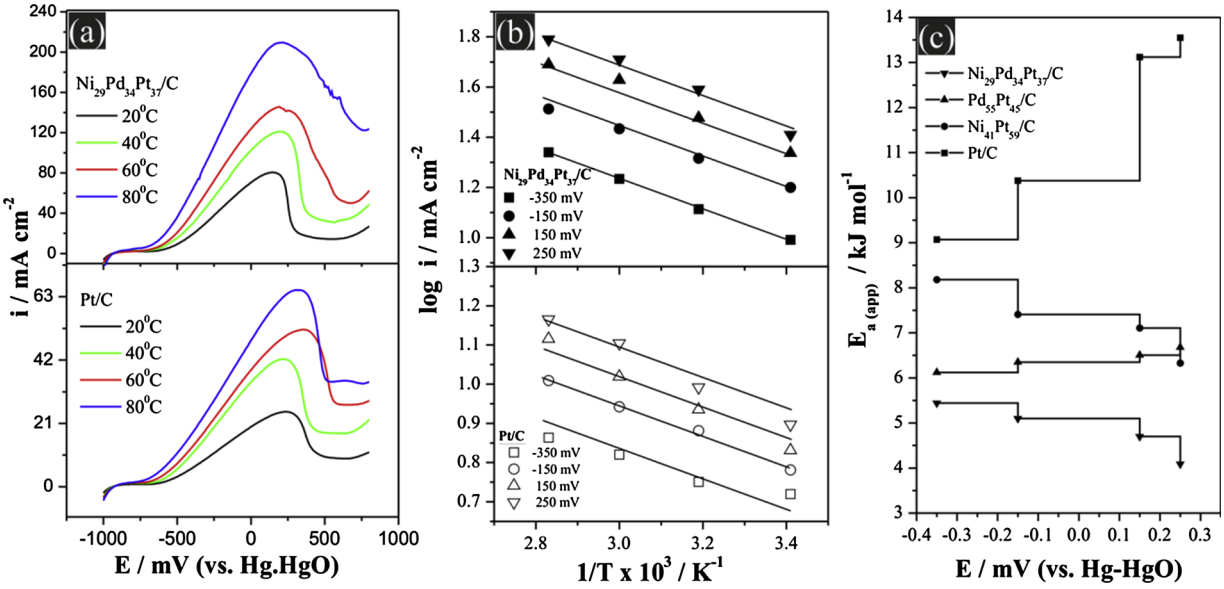

Fig. 7. (a) Linear sweep voltammograms representing the enhancement of ethanol oxidation kinetics with temperature, Scan rate $= 5\ mV\ s^{-1}$ (b) Arrhenius plots of ethanol oxidation on Pt and $Ni_{29}Pd_{34}Pt_{37}$ electrodes. (c) Dependence of apparent activation energy of different catalysts at different potentials in a solution of 0.5 M NaOH and 1.0 M ethanol.

0.20 V, the current slowly begins to rise indicating the formation of surface oxides. The position of the oxide reduction peak in the negative going sweep is shifted to lower potentials for electrodes with higher Pd content. The ECSA values of the binary and ternary compositions from the above voltammograms are summarized in Table S1 in the supplementary information. Analyzing the ECSA values, it appears that $Ni_{41}Pt_{59}$/C and $Ni_{29}Pd_{34}Pt_{37}$/C electrodes are far more effective in generating the active sites. The ECSA of the Pd/C electrodes was also determined by the coulombic charge (Q) of the reduction of PdO_x [12,13,22,45] and the charges assumed for PdO monolayer was 405 mC cm^{-2} [46–48]. For PdPt/C catalyst the ECSA was also determined from the columbic charge (Q) corresponding to the oxide reduction peak. In case of NiPt/C catalyst, the charge required for the reduction of PtO ($q_{PtO\text{-}red}$) and NiO ($q_{NiO\text{-}red}$) monolayer were assumed to be 420 and 430 μC cm^{-2} respectively [23,48] and were used to averaging their individual charges for calculating the ECSA. The charge required for the reduction of oxide monolayer of $Ni_{41}Pt_{59}$/C was calculated to be 424.1 μC cm^{-2}. Similarly, for the $Ni_{29}Pd_{34}Pt_{37}$/C ternary alloys, the required charges for the corresponding mono layer reduction were estimated to be 417.8 μC cm^{-2}.The remarkably high ECSA value (69.9 $m^2\ g^{-1}$) for $Ni_{29}Pd_{34}Pt_{37}$/C, (almost 3 times that for Pt/C) is accounted for the uniform distribution of particle size, and extensive reaction sites exposed throughout the matrix.

Fig.6a shows the CVs of ethanol oxidation recorded in the solution containing 1.0 M ethanol and 0.5 M NaOH on $Ni_{29}Pd_{34}Pt_{37}$/C, $Pd_{55}Pt_{45}$/C, $Ni_{41}Pt_{59}$/C, Pt/C at a scan rate of 50 mV s^{-1}. The peak current densities for the respective electrodes as revealed in Fig.6b are 40.1, 79.4, 70.1 and 107.4 mA/cm^2. This shows the exuberant catalytic activity of $Ni_{29}Pd_{34}Pt_{37}$/C, in terms of significantly high anodic current on $Pt_{37}Pd_{34}Ni_{29}$/C catalyst, 167% higher than that of the Pt/C and 55% higher than that of $Ni_{41}Pt_{59}$/C catalyst, justifying the contributory existence of Ni and Pd in the tri-metallic system. Unlike the other catalysts a broad shoulder is formed at the hydrogen desorption region for the $Ni_{29}Pd_{34}Pt_{37}$/C catalyst, as shown in the inset of Fig.6a. As expected the potentio-dynamic polarization plots (Fig. 6e) are negatively shifted in the onset potential region observed for the $Ni_{29}Pd_{34}Pt_{37}$/C catalysts in comparison to other catalysts. The magnitude of this cathodic shift depends on the Pd and Ni content of the ternary catalysts and with the $Ni_{29}Pd_{34}Pt_{37}$/C electro-catalyst displaying the lowest onset potential corresponding to a decrease of ca. 163 mV from that on Pt, which was however not tangible in the voltammetric records. A distinct step down of potential for the $Ni_{29}Pd_{34}Pt_{37}$/C catalyst is observed for the electrocatalysis current (4 mA cm^{-2}) selected beyond the onset potential region (Fig.6c) and the descending order of onset follows $Ni_{29}Pd_{34}Pt_{37}$/C < $Pd_{55}Pt_{45}$/C < $Ni_{41}Pt_{59}$/C < Pt/C. The catalytic superiority based on the polarization performances is found to be in the order: $Ni_{29}Pd_{34}Pt_{37}$/C, > $Pd_{55}Pt_{45}$/C > $Ni_{41}Pt_{59}$/C > Pt/C. The catalytic preeminence of $Ni_{29}Pd_{34}Pt_{37}$/C is therefore recognized through the minimum requirement of over potential for the EOR kinetics compared to the binary catalysts, as because the co-metal partnership of Pd, Ni with Pt in the trimetallic ensemble presumably reduces the activation energy of the oxidation process. These polarization measurements (Fig.6e) were further complemented by corresponding Tafel analysis, whereby a direct assessment of onset potentials and electrochemical parameters was furnished. Fig.6f shows representative Tafel plots corresponding to the polarization studies. Although the linear region is not wide in all cases, it seems reasonable to state that the Tafel slopes when recorded at potential below −0.2 V are distributed in the range, 252 mV dec^{-1} (for Pt/C) to 181 mV dec^{-1} (for $Ni_{29}Pd_{34}Pt_{37}$/C) as the highest and lowest values respectively. The increase in the Tafel slopes with rise in potential possibly indicates the increased resistance to the dissociative adsorption of ethanol molecule on Pt, being most susceptible to poisoning during the reaction sequence. In order to evaluate the activation parameters, linear sweep voltammograms (LSV) were recorded at the slowest scan rate ($5mVs^{-1}$) in 1.0 M ethanol and 0.5 M NaOH solution on different synthesized catalyst in the temperature range 20–80 °C, as depicted in Fig. 7a. The linearity of the plots and consistency of the slopes indicate unaltered mechanistic pathway regardless of the temperature variation (Fig. 7b). Fig.7 highlights the much lower value of the apparent activation energies, E_a, in the potential range of –0.35 to 0.25 V obtained with $Ni_{29}Pd_{34}Pt_{37}$/C compared to the other catalysts. This effect may be viewed as a manifestation of the kinetic competence brought by the synergistic effort of Pd and Ni in the Pt matrix. The Pt/C exhibits almost a linear rise in E_a values within 9.1 to 14 kJ mol^{-1} with increase of potential from –0.35 to 0.25 V whereas $Ni_{29}Pd_{34}Pt_{37}$/C maintain a low range of E_a values from 5.6–3.9 kJ mol^{-1} in the above potential range (Fig.7c). Some common electrochemical renditions seem to be liable for the E_a pattern for Pt/C and the ternary catalyst in the lower potential region. It is known that ethanol adsorption takes place mainly on Pt sites and Pt surface gets

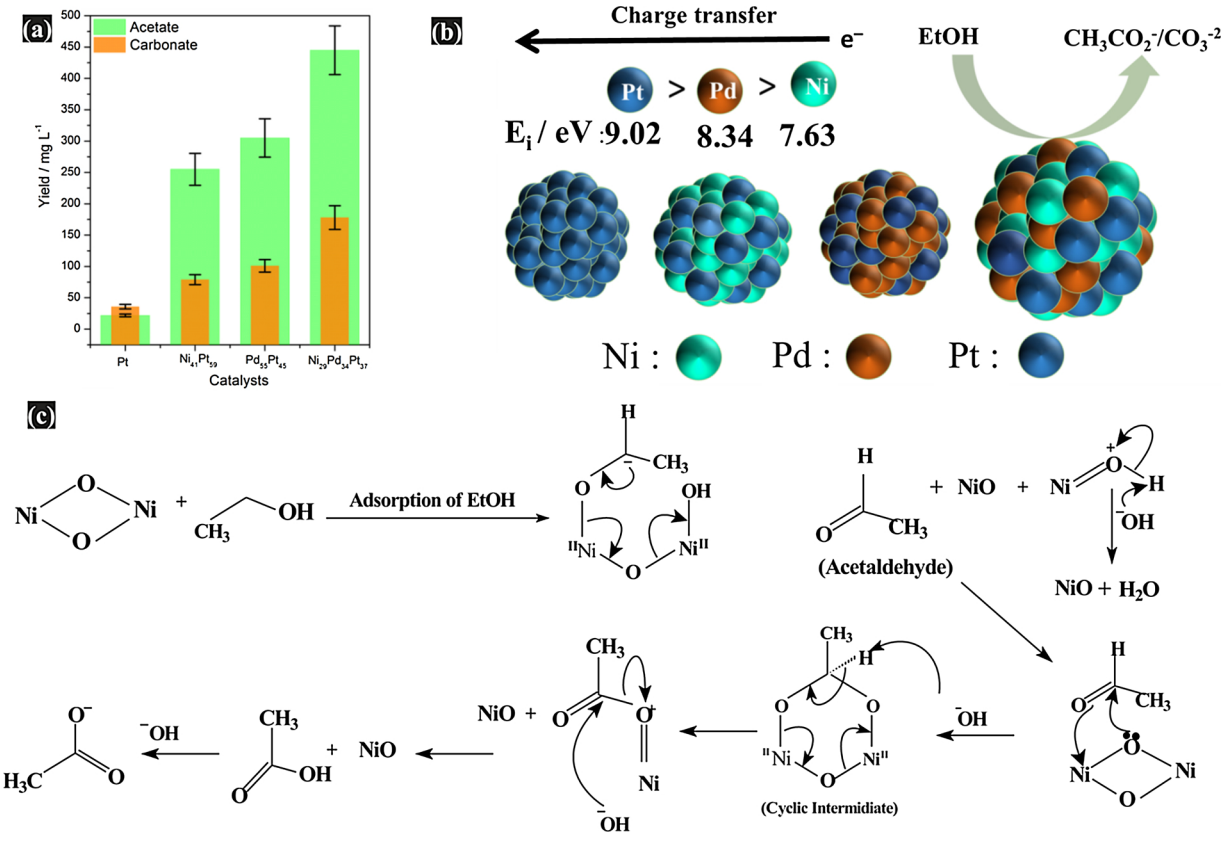

Fig. 8. (a) Yield of acetate and carbonate estimated (in bar diagram) by ion chromatography during the electro-oxidation of ethanol in 0.5 M NaOH on ternary, binary and unary catalysts. (b) Schematic representation of the charge distribution on $Ni_{29}Pd_{34}Pt_{37}$ catalyst. (c) Suggested mechanism for EOR on the ternary catalyst surface ($Ni_{29}Pd_{34}Pt_{37}$) enriched with Ni/NiO/Ni(OH)$_2$.

readily poisoned by adsorbed CO species. These adsorbed species essentially impede the ethanol chemisorption. However, accelerated catalysis is only revived at higher potential due to Pt-O formation. The decrease of free Pt sites would result in the shift of the rate determining step (rds) of ethanol electro-oxidation process to the chemisorption step which is reflected in the increase in apparent activation energy values of Pt/C. On the other hand, highly improved catalytic behavior is shown by the multi-metallic $Ni_{29}Pd_{34}Pt_{37}$/C, as reflected in the significant lowering of E_a values even at low potentials and which strongly indicate to the multi-coupled catalytic effort of the ternary catalysts in executing the entire reaction scheme with less potential input but more energy extraction.

The EOR products were analyzed through ion chromatography under constant potential (−300 mV vs Hg.HgO) on the unary (Pt/C), binary ($Pd_{55}Pt_{45}$, $Ni_{14}Pt_{59}$) and ternary ($Ni_{29}Pd_{34}Pt_{37}$) electrodes for a period of 1 h at the room temperature. The estimated values of the product formed are plotted in Fig. 8a. The yields of the EOR products, acetate and carbonates, were increased with the incorporation of Pd and Ni into the Pt matrix and the highest level for each of the products, is obtained with $Ni_{29}Pd_{34}Pt_{37}$/C catalyst, which corroborates with the electrochemical results. However, it can be predicted from Fig. 8a that the electro-catalysis primarily follows the acetate pathway which is the usual observation with Pt and PdPt combinations in the matrix [29,49,50]. In alkaline medium, Pd surface gets activated with $(OH)_{ads}$ which catalyses the dissociative adsorption of the intermediates so that EOR proceeds in the forward direction. However, the strong adsorption of OH on the catalyst surface at higher potentials may prohibit the reactant molecules to come to the surface and thus inhibit further oxidation of ethanol. This is substantiated by the unusual lift in the peak potential values for the NiPdPt/C catalysts demonstrated in Fig. 6a. On the other hand the ad-atoms synergy is well recognized when the EOR is accelerated over the tri-metallic combination of Pd and Ni with Pt. Here Ni plays a significant role in multiple ways: (i) There is probable electron transfer from Ni to Pt in Pt–Ni and from Pd to Pt in Pd-Pt and Ni to Pt via Pd in Ni-Pd-Pt attributable to the ionization potential values of Ni (7.63 eV), Pd (8.34 eV) and Pt (9.02 eV) as shown in Fig.8b.The process of the partial electron transition between the partnering atoms (Pd, Ni and Pt) in the crystallites, in turn promotes oxide formation in the Ni sites and enables oxidative removal of CO from Pt sites, thus activating Pd to proceed toward ultimate reaction product formation. The electron transfer may contribute to the weakening of Pt−CO bond and enhance the CO_2 formation. *(ii) The Ni oxides/hydroxide layer formed on the Ni–Pd–Pt surface improves the functional properties of the catalysts particles,* such as proton and electron transport and might also protect the bulk material from corrosion attack under ethanol electro-oxidation conditions. The oxygen-containing species therefore impart high catalytic activity on Ni–Pd–Pt alloy for EOR by transforming CO-like poisoning species on Pt into CO_2, leaving the active Pt sites free for further anchorage of ethanol molecules. The presence of Ni $(OH)_2$ on NiPt and NiPdPt surfaces is also expected to facilitate the ethanol oxidation by increasing OH^- concentration at lower potential range resulting in decrease of over potential of the reaction as shown in Fig.6a and d. It is also well known that Ni can produce surplus OH via auto-catalytic reaction in alkaline condition and at a potential much below -0.7 V (Ni $(OH)_2 \rightarrow$NiO + H_2O; Ni $(OH)_2 \rightarrow$NiOOH + H+ e^-) [23,28,45,51].

The EOR sequences involve the intervention of NiOOH and Ni, particularly in the dimeric form of $(NiO)_2$ [52] as reported in our earlier work [23], initiating the reaction to a significant amount acetate formation (Fig. 8c) in one hand and simultaneous propagation toward carbonate formation to considerable extent. Moreover, it is also important that Pd content of ~40–50% becomes critical for the

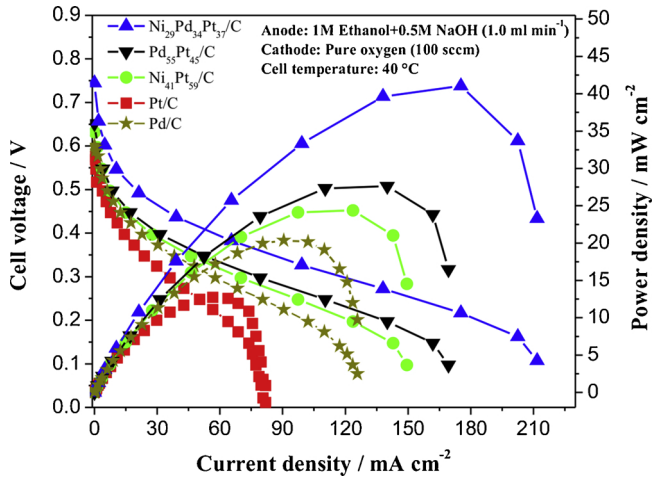

Fig. 9. Polarization and power-density curves of the DE (AEM)FC with ternary $Ni_{29}Pd_{34}Pt_{37}$, binary$Ni_{41}Pt_{59}$, $Pd_{55}Pt_{45}$, and unary Pd/C, Pt/C, electrodes (anode: 0.5 M NaOH 1.0 M ethanol) at 40 °C.

satisfactory propagation of EOR in alkaline medium. This is also congruent with the earlier observations whenever Pd has been one of the component metals in the multi-metallic matrices. On the other hand, the optimum level of Ni in the co-metals ensemble becomes a key factor in generating the maximum peak current density for EOR and seemingly, the highest current output is delivered by the catalyst having 29% Ni co-existing with Pd and Pt in the matrix. It also appears that the tri-metallic partnership in the proportions ~1:1:1 ($Ni_{29}Pd_{34}Pt_{37}$/C), *i.e* with almost ~ 30% share of Ni, is responsible for triggering the kinetics to its highest level.

The polarization and power density curves of alkaline DEFCs using Pt/C, NiPt/C and Ni-Pd-Pt/C as the anode catalyst [53] fabricated in an in-house AEM-DEFC are presented in Fig.9. The OCV (0.74 V) is found to be higher by 0.17 V than the value obtained with Pt/C, which is consistent with the onset potential of EOR in CV characterization. The measurements were made by feeding 1.0 M ethanol mixed with 0.5 M KOH to the fuel cell at 40 °C. Much better power characteristics were derived from the alkaline DEFC with $Ni_{29}Pd_{34}Pt_{37}$/C anode producing OCV 0.76 V and power density 41 mW cm^{-2} while that for Pt/C is 12 $mWcm^{-2}$; the former being 241% higher than the latter. On the other hand, the peak power density generated from $Ni_{29}Pd_{34}Pt_{37}$/C is almost 51% and 78% greater than the respective binary catalysts $Pd_{55}Pt_{45}$/C and $Ni_{41}Pt_{59}$/C. Thus the ternary $Ni_{29}Pd_{34}Pt_{37}$/C anode catalyst with much reduced loading of Pt and Pd, appears to be more efficient in energy extraction than the unary and also the binary counterparts, in terms of both open-circuit voltage (OCV) and power density.

3. Conclusion

Enhanced electro-catalytic activity of carbon supported binary alloyed nano-particles; NiPt and ternary NiPdPt/C were synthesized by one pot $NaBH_4$ reduction method and investigated for the electro-catalysis in alkaline ethanol solutions. The NiPdPt/C nano-catalysts displays all the electro-catalytic features like peak current density, onset potential, estimated oxidation products, OCV, and power density, superior to that of pure Pt/C, PdPt/C and NiPt/C binary catalyst. It has been suggested that the presence of Ni and its oxide and hydroxide not only substantiate Pd effect by supplying surplus OH through the NiOOH spices in high pH condition, but also triggers the C—C bond scission during the dissociative adsorption of ethanol.

Acknowledgement

The authors gratefully acknowledge the support from Central of Scientific and Industrial Research (CSIR), New Delhi, India. Support by the CTI Swiss Competence Center for Energy Research (SCCER Heat and Electricity Storage) projects at Department of Chemistry and Biochemistry, University of Bern, Bern, Switzerland is gratefully acknowledged. P.B. acknowledges financial support from the Swiss National Science Foundation (grant No. 200020–172507)

Appendix A. Supplementary data

Supplementary material related to this article can be found, in the online version, at doi:https://doi.org/10.1016/j.apcatb.2019.117847.

References

[1] A. Holewinski, J.-C. Idrobo, S. Linic, High-performance Ag–Co alloy catalysts for electrochemical oxygen reduction, Nat. Chem. 6 (2014) 828.
[2] C. Sealy, The problem with platinum, Mater. Today 11 (2008) 65–68.
[3] M.S. Saha, V. Neburchilov, D. Ghosh, J. Zhang, Nanomaterials-supported Pt catalysts for proton exchange membrane fuel cells, Wiley Interdiscip. Rev. Energy Environ. 2 (2013) 31–51.
[4] M.J. Lee, J.S. Kang, Y.S. Kang, D.Y. Chung, H. Shin, C.-Y. Ahn, S. Park, M.-J. Kim, S. Kim, K.-S. Lee, Y.-E. Sung, Understanding the bifunctional effect for removal of CO poisoning: blend of a platinum nanocatalyst and hydrous ruthenium oxide as a model system, ACS Catal. 6 (2016) 2398–2407.
[5] J. Li, S. Ghoshal, M.K. Bates, T.E. Miller, V. Davies, E. Stavitski, K. Attenkofer, S. Mukerjee, Z.F. Ma, Q. Jia, Experimental proof of the bifunctional mechanism for the hydrogen oxidation in alkaline media, Angew. Chem. Int. Ed. 56 (2017) 15594–15598.
[6] T. Wu, J. Fan, Q. Li, P. Shi, Q. Xu, Y. Min, Palladium nanoparticles anchored on anatase titanium dioxide-black phosphorus hybrids with heterointerfaces: highly electroactive and durable catalysts for ethanol electrooxidation, Adv. Energy Mater. 8 (2018) 1701799.
[7] J. Mao, W. Chen, D. He, J. Wan, J. Pei, J. Dong, Y. Wang, P. An, Z. Jin, W. Xing, H. Tang, Z. Zhuang, X. Liang, Y. Huang, G. Zhou, L. Wang, D. Wang, Y. Li, Design of ultrathin Pt-Mo-Ni nanowire catalysts for ethanol electrooxidation, Sci. Adv. 3 (2017).
[8] A. Dutta, C.E. Morstein, M. Rahaman, A. Cedeño López, P. Broekmann, Beyond copper in CO2 electrolysis: effective hydrocarbon production on silver-nanofoam catalysts, ACS Catal. 8 (2018) 8357–8368.
[9] A. Kowal, M. Li, M. Shao, K. Sasaki, M.B. Vukmirovic, J. Zhang, N.S. Marinkovic, P. Liu, A.I. Frenkel, R.R. Adzic, Ternary Pt/Rh/SnO2 electrocatalysts for oxidizing ethanol to CO2, Nat. Mater. 8 (2009) 325.
[10] L.S. Parreira, J.C.M. Silva, F.R. Simões, M.A.L. Cordeiro, R.H. Sato, E.R. Leite, M.Cd. Santos, PtSn electrocatalyst supported on MWCNT-COOH: investigating the ethanol oxidation reaction, Chem. Electro. Chem. 4 (2017) 1950–1958.
[11] X. Cao, N. Wang, Y. Han, C. Gao, Y. Xu, M. Li, Y. Shao, PtAg bimetallic nanowires: facile synthesis and their use as excellent electrocatalysts toward low-cost fuel cells, Nano Energy 12 (2015) 105–114.
[12] J. Datta, A. Dutta, S. Mukherjee, The beneficial role of the cometals Pd and Au in the carbon-supported PtPdAu catalyst toward promoting ethanol oxidation kinetics in alkaline fuel cells: temperature effect and reaction mechanism, J. Phys. Chem. C 115 (2011) 15324–15334.
[13] A. Dutta, J. Datta, Outstanding catalyst performance of PdAuNi nanoparticles for the anodic reaction in an alkaline direct ethanol (with anion-exchange membrane) fuel cell, J. Phys. Chem. C 116 (2012) 25677–25688.
[14] S. Gottesfeld, D.R. Dekel, M. Page, C. Bae, Y. Yan, P. Zelenay, Y.S. Kim, Anion exchange membrane fuel cells: current status and remaining challenges, J. Power Sources 375 (2018) 170–184.
[15] W. Huang, H. Wang, J. Zhou, J. Wang, P.N. Duchesne, D. Muir, P. Zhang, N. Han, F. Zhao, M. Zeng, J. Zhong, C. Jin, Y. Li, S.-T. Lee, H. Dai, Highly active and durable methanol oxidation electrocatalyst based on the synergy of platinum–nickel hydroxide–graphene, Nat. Commun. 6 (2015) 10035.
[16] X. Zhao, S. Chen, Z. Fang, J. Ding, W. Sang, Y. Wang, J. Zhao, Z. Peng, J. Zeng, Octahedral Pd@Pt1.8Ni core–Shell nanocrystals with ultrathin PtNi alloy shells as active catalysts for oxygen reduction reaction, J. Am. Chem. Soc. 137 (2015) 2804–2807.
[17] A. Dutta, J. Ouyang, Ternary NiAuPt nanoparticles on reduced graphene oxide as catalysts toward the electrochemical oxidation reaction of ethanol, ACS Catal. 5 (2015) 1371–1380.
[18] D. Soundararajan, J.H. Park, K.H. Kim, J.M. Ko, Pt–Ni alloy nanoparticles supported on CNF as catalyst for direct ethanol fuel cells, Curr. Appl. Phys. 12 (2012) 854–859.
[19] A. Dutta, A. Mondal, J. Datta, Tuning of platinum nano-particles by Au usage in their binary alloy for direct ethanol fuel cell: controlled synthesis, electrode kinetics and mechanistic interpretation, J. Power Sources 283 (2015) 104–114.
[20] J. Zhang, I. Yazgan, V.M. Kariuki, O.A. Sadik, Poly (Amic) acid improves the efficiency and stability of PtCr nanoparticle catalyst during ethanol oxidation reaction, J. Electrochem. Soc. 164 (2017) H701–H706.
[21] S.Y. Shen, T.S. Zhao, J.B. Xu, Y.S. Li, Synthesis of PdNi catalysts for the oxidation of ethanol in alkaline direct ethanol fuel cells, J. Power Sources 195 (2010) 1001–1006.

[22] C. Xu, Z. Tian, P. Shen, S.P. Jiang, Oxide (CeO2, NiO, Co3O4 and Mn3O4)-promoted Pd/C electrocatalysts for alcohol electrooxidation in alkaline media, Electrochim. Acta 53 (2008) 2610–2618.
[23] A. Dutta, J. Datta, Energy efficient role of Ni/NiO in PdNi nano catalyst used in alkaline DEFC, J. Mater. Chem.A 2 (2014) 3237–3250.
[24] B. Pierozynski, T. Mikolajczyk, Enhancement of ethanol oxidation reaction on Pt (PtSn)-Activated nickel foam through in situ formation of nickel oxy-hydroxide layer, Electrocatalysis 8 (2017) 252–260.
[25] S. Sarkar, R. Jana, H. Vadlamani, S. Ramani, D. Mumbaraddi, S.C. Peter, Facile aqueous-phase synthesis of the PtAu/Bi2O3 hybrid catalyst for efficient electrooxidation of ethanol, ACS Appl. Mater. Interfaces 9 (2017) 15373–15382.
[26] Z. Cao, Q. Chen, J. Zhang, H. Li, Y. Jiang, S. Shen, G. Fu, B.-a. Lu, Z. Xie, L. Zheng, Platinum-nickel alloy excavated nano-multipods with hexagonal close-packed structure and superior activity towards hydrogen evolution reaction, Nat. Commun. 8 (2017) 15131.
[27] V.R. Stamenkovic, B. Fowler, B.S. Mun, G. Wang, P.N. Ross, C.A. Lucas, N.M. Marković, Improved oxygen reduction activity on Pt&sub&3&/sub&Ni(111) via increased surface site availability, Science 315 (2007) 493.
[28] M. Martins, B. Šljukić, C.A.C. Sequeira, G.S.P. Soylu, A.B. Yurtcan, G. Bozkurt, T. Sener, D.M.F. Santos, PtNi supported on binary metal oxides: Potential bifunctional electrocatalysts for low-temperature fuel cells? Appl. Surf. Sci. 428 (2018) 31–40.
[29] Y. Zhai, Z. Zhu, X. Lu, Z. Zhou, J. Shao, H.S. Zhou, Facile synthesis of three-dimensional PtPdNi fused nanoarchitecture as highly active and durable electrocatalyst for methanol oxidation, Acs Appl. Energy Mater. 1 (2018) 32–37.
[30] H. Liao, A. Fisher, Z.J. Xu, Surface segregation in bimetallic nanoparticles: a critical issue in electrocatalyst engineering, Small 11 (2015) 3221–3246.
[31] Z. Qi, H. Geng, X. Wang, C. Zhao, H. Ji, C. Zhang, J. Xu, Z. Zhang, Novel nanocrystalline PdNi alloy catalyst for methanol and ethanol electro-oxidation in alkaline media, J. Power Sources 196 (2011) 5823–5828.
[32] J.E. Sulaiman, S. Zhu, Z. Xing, Q. Chang, M. Shao, Pt–Ni Octahedra as electrocatalysts for the ethanol electro-oxidation reaction, ACS Catal. 7 (2017) 5134–5141.
[33] W.J. Zhou, S.Q. Song, W.Z. Li, G.Q. Sun, Q. Xin, S. Kontou, K. Poulianitis, P. Tsiakaras, Pt-based anode catalysts for direct ethanol fuel cells, Solid State Ion. 175 (2004) 797–803.
[34] S. Tanaka, M. Umeda, H. Ojima, Y. Usui, O. Kimura, I. Uchida, Preparation and evaluation of a multi-component catalyst by using a co-sputtering system for anodic oxidation of ethanol, J. Power Sources 152 (2005) 34–39.
[35] Z.B. Wang, G.P. Yin, P.F. Shi, Y.C. Sun, Novel Pt–Ru–Ni/C catalysts for methanol electro-oxidation in acid medium, Electrochem. Solid-State Lett. 9 (2006) A13–A15.
[36] L. An, T.S. Zhao, An alkaline direct ethanol fuel cell with a cation exchange membrane, Energy Environ. Sci. 4 (2011) 2213–2217.
[37] S. Shen, T.S. Zhao, J. Xu, Y. Li, High performance of a carbon supported ternary PdIrNi catalyst for ethanol electro-oxidation in anion-exchange membrane direct ethanol fuel cells, Energy Environ. Sci. 4 (2011) 1428–1433.
[38] K. Jayasayee, J.A.R. Van Veen, E.J.M. Hensen, F.A. de Bruijn, Influence of chloride ions on the stability of PtNi alloys for PEMFC cathode, Electrochim. Acta 56 (2011) 7235–7242.
[39] P. Mani, R. Srivastava, P. Strasser, Dealloyed binary PtM3 (M = Cu, Co, Ni) and ternary PtNi3M (M = Cu, Co, Fe, Cr) electrocatalysts for the oxygen reduction reaction: performance in polymer electrolyte membrane fuel cells, J. Power Sources 196 (2011) 666–673.
[40] K.-W. Park, J.-H. Choi, B.-K. Kwon, S.-A. Lee, Y.-E. Sung, H.-Y. Ha, S.-A. Hong, H. Kim, A. Wieckowski, Chemical and electronic effects of Ni in Pt/Ni and Pt/Ru/Ni alloy nanoparticles in methanol electrooxidation, J. Phys. Chem. B 106 (2002) 1869–1877.
[41] A. Dutta, A. Mondal, P. Broekmann, J. Datta, Optimal level of Au nanoparticles on Pd nanostructures providing remarkable electro-catalysis in direct ethanol fuel cell, J. Power Sources 361 (2017) 276–284.
[42] G.-j. Wang, Y.-z. Gao, Z.-b. Wang, C.-y. Du, J.-j. Wang, G.-p. Yin, Investigation of PtNi/C anode electrocatalysts for direct borohydride fuel cell, J. Power Sources 195 (2010) 185–189.
[43] M. Rahaman, A. Dutta, P. Broekmann, Size-dependent activity of palladium nanoparticles: efficient conversion of CO2 into formate at low overpotentials, ChemSusChem 10 (2017) 1733–1741.
[44] S.L. Bergman, J. Granestrand, Y. Tang, R.S. París, M. Nilsson, F.F. Tao, C. Tang, S.J. Pennycook, L.J. Pettersson, S.L. Bernasek, In-situ characterization by Near-Ambient Pressure XPS of the catalytically active phase of Pt/Al2O3 during NO and CO oxidation, Appl. Catal. B 220 (2018) 506–511.
[45] S.Y. Shen, T.S. Zhao, J.B. Xu, Y.S. Li, Synthesis of PdNi catalysts for the oxidation of ethanol in alkaline direct ethanol fuel cells, J. Power Sources 195 (2010) 1001–1006.
[46] A.N. Geraldes, D.F. da Silva, E.S. Pino, J.C.M. da Silva, R.F.B. de Souza, P. Hammer, E.V. Spinacé, A.O. Neto, M. Linardi, M.C. dos Santos, Ethanol electro-oxidation in an alkaline medium using Pd/C, Au/C and PdAu/C electrocatalysts prepared by electron beam irradiation, Electrochim. Acta 111 (2013) 455–465.
[47] Q. He, W. Chen, S. Mukerjee, S. Chen, F. Laufek, Carbon-supported PdM (M = Au and Sn) nanocatalysts for the electrooxidation of ethanol in high pH media, J. Power Sources 187 (2009) 298–304.
[48] A. Dutta, J. Datta, Significant role of surface activation on Pd enriched Pt nano catalysts in promoting the electrode kinetics of ethanol oxidation: temperature effect, product analysis & theoretical computations, Int. J. Hydrogen Energy 38 (2013) 7789–7800.
[49] D. Basu, S. Basu, Performance studies of Pd–Pt and Pt–Pd–Au catalyst for electrooxidation of glucose in direct glucose fuel cell, Int. J. Hydrogen Energy 37 (2012) 4678–4684.
[50] Y.-H. Cho, B. Choi, Y.-H. Cho, H.-S. Park, Y.-E. Sung, Pd-based PdPt (19: 1)/C electrocatalyst as an electrode in PEM fuel cell, Electrochem. commun. 9 (2007) 378–381.
[51] Y.-Y. Zhou, C.-H. Liu, J. Liu, X.-L. Cai, Y. Lu, H. Zhang, X.-H. Sun, S.-D. Wang, Self-decoration of PtNi alloy nanoparticles on multiwalled carbon nanotubes for highly efficient methanol electro-oxidation, Nano-micro Lett. 8 (2016) 371–380.
[52] M.M. Natile, A. Glisenti, Surface reactivity of NiO: interaction with methanol, Chem. Mater. 14 (2002) 4895–4903.
[53] A. Dutta, J. Ouyang, Enhanced electrocatalytic performance on polymer-stabilized graphene decorated with alloy nanoparticles for ethanol oxidation reaction in alkaline media, Appl. Catal. B: Environ. 158 (2014) 119–128.